Solid Freeform Fabrication 2024: Proceedings of the 35th Annual International Solid Freeform Fabrication Symposium – An Additive Manufacturing Conference
Reviewed Paper

Effects of Powder Characteristics of Different Alloy Powders on Part Quality in Area Printing® Additive Manufacturing

B. Fotovvati, T-N. Le, N. Ferreri, S. Shrestha, and N. Duanmu

Seurat Technologies Inc., Wilmington, MA, USA 01887

Abstract

As laser powder bed fusion (LPBF) technology has transitioned from prototyping to end-use parts, understanding the role of the powder properties needed to reliably produce parts of acceptable quality becomes critical. In this study, different alloy powders from different manufacturers are tested for flowability, spreadability, tapped density, particle size distribution, and morphology using scanning electron microscopy (SEM). The tested alloys include stainless-steel 316L, Nickel-based super alloy 625 (IN625), M300 maraging steel (also known as Tool Steel 1.2709 and 18Ni300), and AlSi10Mg. These powders were then used as feedstock in the Area Printing process to print density cubes with a wide range of laser parameters to correlate the powder characteristics with part density. The results suggest a strong correlation between these characteristics and the density of the parts as well as among the powder characteristics themselves.

Keywords: Additive Manufacturing; Laser Powder Bed Fusion; Area Printing; Particle Size Distribution; Flowability; Cohesive Index; Machine Learning

1. Introduction

Laser-based Powder Bed Fusion (LPBF), also referred to as Selective Laser Melting (SLM) or Direct Metal Laser Sintering (DMLS), is among the most prevalent methods of metal additive manufacturing (AM). This technique involves the selective melting of metal powders in a layer-by-layer process using a high-intensity laser beam, guided by a segmented computer-aided design (CAD) model. LPBF finds extensive applications across several industries, such as medical, automotive, and aerospace sectors [1]. The widespread adoption of this manufacturing technique in these industries is attributed to its numerous advantages, including design flexibility, shortened production times, minimized material waste, and sustainability benefits. However, the limited production rate of LPBF, along with its high capital and operational costs, has hindered its broader adoption compared to traditional manufacturing methods. To overcome this limitation, Seurat Technologies has introduced Large-Area Pulsed Laser Powder Bed Fusion (LAPBF), also known as "Area Printing." This innovative approach replaces the conventional point laser with a large-area pulsed laser, capable of melting metal over several millimeters in a single pulse, with a repetition rate of up to 40 Hz. This advancement can significantly reduce manufacturing time and lower final production costs. Additionally, the large-area laser beam mitigates spattering issues common in conventional LPBF by avoiding the creation of a deep, turbulent melt pool (keyhole) that generates strong recoil pressures and ejects spatters [2].

One of the most critical factors determining the quality of the manufactured components in both the LPBF process and the Area Printing process is the properties of the powder feedstock [3]. Brika et al. [4] reported that Ti6Al4V powder characteristics, including size distribution and sphericity, significantly affect the rheological behavior and packing density of the feedstock. Consequently, these characteristics influence the quality of the built parts, including density, surface finish, and dimensional accuracy. Similarly, for 316L stainless steel, Groarke et al. [5] unveiled the strong correlation between the particle size and shape parameters and the powder rheology. The authors in [5] also reported the effects of powder size distribution on the microstructure and the mechanical properties of the fabricated parts. Furthermore, Mussatto et al. [6] demonstrated that powder rheological properties, particularly spreadability, play a crucial role in determining both the thickness of the powder layer and the parameters governing spreading, such as mechanism and speed. Spurek et al. [7] studied the impact of powder particle sizes on melt pool dimensions and part density. The authors observed an inverse relationship between the median particle size and part density, although they found no correlation with the distribution width. It is likely that fluctuations in melt pool depth and width significantly influence part density [7]. Specifically, increasing the median particle size tends to decrease melt pool depth while increasing width fluctuations [7]. Regarding the effects of particle sizes in the LPBF process of IN625, Pleass et al. [8] concluded that an increase in the number of particles with diameters less than 10 μm negatively impacts the spreadability of the feedstock. This is attributed to the overwhelming cohesive forces when the D90 is less than 10 μm [8]. To elucidate the correlation between powder flowability and the spreadability of Ti6Al4V powder, Mehrabi et al. [9] conducted both flowability and spreadability tests for two different grades of powders. The authors reported that a higher spreadability index can be quantitatively achieved with increased flowability. Averardi et al. [10] emphasized that the density of the built part can be significantly improved by increasing the powder bed packing density using various powder size distributions and shapes for the powder feedstock.

In this study, various alloy powders sourced from different manufacturers were systematically evaluated for their flowability, spreadability, particle size distribution, and morphology. Scanning electron microscopy (SEM) was employed to analyze the morphology of the powders. The alloys tested in this investigation included stainless-steel 316L, Nickel-based superalloy 625 (Inconel 625), M300 maraging steel (also referred to as Tool Steel 1.2709 and 18Ni300), AlSi10Mg, and Ti6Al4V. Subsequently, these powders were utilized as feedstock in the Area Printing process to fabricate density cubes. A wide range of laser parameters was employed during the printing process to establish a correlation between the inherent characteristics of the powders and the resulting density of the printed parts. By examining the interplay between powder properties and part density, this study aims to provide valuable insights into optimizing additive manufacturing processes for enhanced material performance and structural integrity. In addition, the effects of powder recyclability on the quality and properties of the feedstock and the built parts density are also investigated.

2. Materials and Methods

Different alloy powders from various manufacturers were tested and then used as feedstock in the Area Printing process to print density cubes using a wide range of laser parameters. This approach aimed to correlate powder characteristics with part density. Each density build included 49 cubes. To develop a material-independent methodology, this study included a variety of materials based on availability. The tested powders comprised stainless-steel 316L from nine different suppliers, Nickel-based super alloy 625 (Inconel 625) from eight different suppliers, M300 maraging steel (also known as Tool Steel 1.2709 and 18Ni300) from seven different suppliers, and AlSi10Mg from six different suppliers. The following sub-sections detail the testing and fabrication processes.

2.1. Powder Characterizations

The elemental compositions of the powders were determined using energy dispersive spectroscopy (EDS) with a TESCAN LYRA3 GMU SEM. Particle size distribution (PSD) and morphology were analyzed using a Microtrac MRB. Spreadability-related properties, including the cohesive index, roughness index, aeration, and dynamic angle of repose, were measured using a GranuDrum. The GranuDrum operates by rotating a drum filled with powders, analyzing their flowability and rheological properties through image capture and processing of the material's behavior during rotation. Tapped density and the Hausner ratio were measured and calculated using an Autotap tapped density tester. Additionally, Hall and Carney funnels were employed to measure the powders' flowability. Figure 1 shows some of the powder testing equipment.

Figure 1. From left to right: Microtrac MRB, GranuDrum, and Autotap tapped density tester.

2.2. Area Printing

Each batch of powders from each material was used separately to fabricate density cubes using Area Printing. In this process, two types of lasers are utilized to melt metal powder layers and fuse them to the area below it, manufacturing entire renderings at once in a single defined area. A set of diode lasers is used to preheat and sinter the powder bed before a single Nd:YAG pulsed laser performs the final melting of the area. Figure 2 illustrates a schematic of the pulsed laser beam from the source to the powder bed. Once the laser is created, it is shaped into a homogeneous square field called a "tile". A blue light projector then generates a projection of the area pattern the same size as the square laser beam, which is aligned with the laser beam. An Optically Addressable Light Valve (OALV) receives this light and horizontally polarizes the laser beam where blue and IR light pixels overlap and vertically polarizes them where they do not overlap. The vertically and horizontally polarized laser beams are then split, and the resulting area pattern is sent through a scanner system to the powder bed to melt the patterned field.

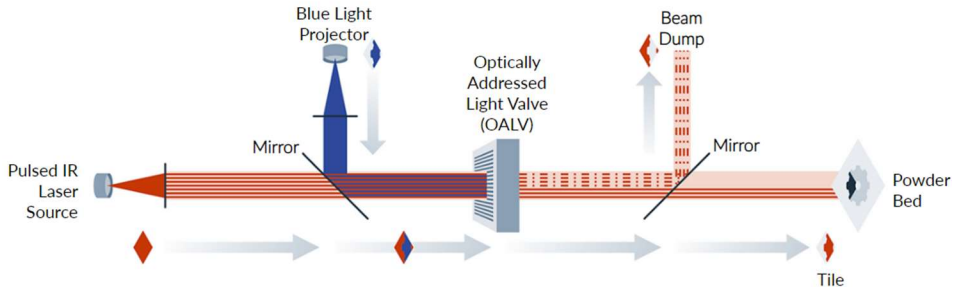

Figure 2. Schematic of the pulsed laser beam used in the Area Printing process [11].

2.3. Part Density Measurements

Experiments were conducted using stainless steel 316L, IN625, M300 maraging steel, and AlSi10Mg powders with varying particle size distributions. Each print job consisted of a seven-by-seven grid of cubes with the following dimensions printed on an Area Printing Prototype System. The dimensions are 10 mm x 10 mm x 10 mm for 316L, IN625, and M300 alloys and 12 mm x 12 mm x 25 mm for AlSi10Mg. The consideration of larger AlSi10Mg samples aims to compensate for the material's lower density and ensure sufficient mass to maintain measurement accuracy. Figure 3 shows a batch of SS316L density cubes fabricated by the Seurat prototype printer. Upon completion, the build plate was removed, and the samples were cut from it using a horizontal band saw. The samples were then soaked in isopropanol in an ultrasonic cleaner for 30 minutes prior to density measurements. Density measurements were performed using the Archimedes method with an Ohaus Explorer™ Precision density kit.

Figure 3. SS316L cubes for density measurement on the Seurat prototype machine build plate.

2.4.Data Analysis

The data analysis consists of two main components: identifying correlations among different powder characteristics and predicting the response, specifically porosity, using machine learning (ML) methods. Spearman Rank Correlation was employed to identify two-way correlations among powder characteristics and determine the most significant parameters for predicting porosity. Due to the varying ranges of values among some predictors, normalization was performed before model training. Given the relatively small dataset, Bootstrap Sampling was applied to increase the number of observations and enhance model accuracy. This method involves repeatedly sampling from the original dataset with replacement to estimate population properties and create multiple bootstrap samples. This technique exposed the model to various data distributions, reducing overfitting and improving generalization to unseen data. The Gradient Boosting ML technique was then employed using the bootstrapped dataset for porosity prediction. In this regression method, an ensemble model is built by sequentially adding weak learners, such as decision trees, to correct errors made by previous models. In this study, the model was configured with 500 estimators (decision trees), each with a maximum depth of 5 and a learning rate of 1.0. Gradient descent optimization was employed to minimize the mean squared error (Friedman MSE) loss function. All data analysis was conducted using Python.

3. Results and Discussions

All the experimental results are summarized in Table 1, with the data organized into columns according to the category of properties. Note that EDS analysis was not performed on IN625 powder samples, as indicated by "n/a" in the corresponding cells of the table. Figure 4 illustrates the two-way correlations among powder properties using a Spearman correlation matrix. Due to significant differences in elemental compositions across some alloys and numerous missing data points, reasonable correlations using elemental compositions as predictors could not be achieved in the tested ML models; thus, this category was excluded from the model. On the Spearman correlation matrix, the correlation between every two parameters can be found in the row-column intersection of those two parameters and compared to the other correlations. For instance, PSD parameters, i.e., D10, D50, and D90, are negatively correlated with bulk density, tapped density, Hall, and Carney. It means increasing the powder particle size will decrease the powder density (both bulk and tapped) by introducing larger void spaces in between the particles. It also decreases the flowability values, i.e., the time it takes for 50 grams of powder to flow, which results in increasing the powder flowability, which is consistent with findings in the literature [12]. Another notable example is sphericity, which negatively correlates with the Hausner ratio, where lower Hausner ratios indicate higher compactibility of particles (closer values of bulk and tapped densities). Thus, higher sphericity results in greater compactness of powder particles. Sphericity also negatively correlates with GranuDrum parameters, showing that increased sphericity reduces powder cohesiveness and enhances flowability and spreadability. Additionally, there are strong positive correlations among parameters within the same category, such as Hall and Carney flow rates, and D10, D50, and D90 particle sizes.

Table 1. Dataset obtained by various powder testing and density measurements.

Alloy	Batch	Elemental Composition										Tapped Density (g/cm^3)			Powder Size Distribution					GranuDrum				Flowability (s/50g)		Porosity (%)
		Fe	Cr	Ni	Mo	Mn	Si	Co	Ti	Al	Mg	Bulk Den.	Tap Den.	Hausner	D10 (µm)	D50 (µm)	D90 (µm)	Sphericity	Skewness	Aeration	Angle	Cohesive	Roughness	Hall	Carney	
SS316L	A	62.5	18.7	12.9	2.8	2.2	0.9	0	0	0	0	4.3	4.933	1.147	23.87	36.4	47.31	0.966	0.83	0.92	37.36	11.76	1.17	28.62	4.99	0.05
	B	66.5	16.8	12.3	2.7	1.1	0.7	0	0	0	0	4.132	4.717	1.142	20.53	34.34	45.73	0.964	0.91	1.06	42.74	22.29	1.24	19	4.00	n/a
	C	64.4	17.1	12.9	2.5	2.1	1.0	0	0	0	0	4.467	4.905	1.098	26.22	43.3	59.44	0.965	0.94	1.01	33.89	9.34	1.12	14.89	2.92	0.54
	D	65.0	17.8	12.8	2.1	1.6	0.7	0	0	0	0	4.59	5.105	1.112	17.82	30.12	45.91	0.970	0.59	0.93	35.43	14.01	1.14	18.36	3.2	0.68
	E	66.1	16.7	11.6	2.3	2.2	1.0	0	0	0	0	4.613	5.079	1.101	14	23.91	44.8	0.96	0.70	0.99	32.92	13.8	1.14	18.05	3.09	0.74
	F	65.4	18.2	11.9	1.8	2.3	0.5	0	0	0	0	4.321	4.914	1.137	20.94	33.24	47.17	0.972	0.78	1.00	33.41	12.98	1.14	15.28	3.01	0.38
	G	68.2	17.0	10.5	2.1	1.8	0.4	0	0	0	0	4.097	4.94	1.206	24.6	36.76	50.82	0.944	1.49	0.99	46.82	20.54	1.27	19	4.00	n/a
	H	69.1	16.3	10.6	2.0	1.2	0.7	0	0	0	0	4.287	4.87	1.136	17.49	33.95	53.26	0.967	0.60	0.98	33.66	11.61	1.14	17.97	3.33	0.64
	I	n/a	n/a	n/a	n/a	n/a	n/a	n/a	n/a	n/a	n/a	4.351	4.933	1.134	27.08	39.58	50.32	0.967	1.25	0.92	36.35	18.8	1.17	17.75	2.97	n/a
AlSi10Mg	A	0.2	0	0	0	0	9.4	0	0.1	89.3	1.0	1.442	1.654	1.148	27.46	44.95	61.95	0.965	1.16	1.02	36.2	21.08	1.2	15.32	2.82	0.28
	B	0.1	0	0	0	0	10.2	0	0.1	88.5	1.1	1.39	1.696	1.22	29.48	49.66	72.93	0.949	0.9	1.03	38.12	23.18	1.21	18.08	3.29	0.6
	C	0.2	0	0	0	0	8.9	0	0.1	89.7	1.1	1.451	1.697	1.169	32.21	49.99	67.8	0.963	1.14	0.97	34	12.95	1.16	16.34	3.05	0.67
	D	0.2	0	0	0	0	9.2	0	0.1	89.4	1.1	1.516	1.696	1.119	31.04	46.86	63.18	0.973	0.92	0.97	32.64	11.89	1.14	13.7	2.56	0.47
	E	0.1	0	0	0	0	12.4	0	0.3	86.0	1.2	1.496	1.671	1.117	39.46	59.07	75.87	0.977	1.4	0.98	31.14	11.12	1.13	16.09	3.01	0.8
	F	0.1	0	0	0	0	16.8	0	0.2	81.1	1.8	1.524	1.734	1.138	21.78	31.37	40.75	0.979	0.93	0.96	33.24	22.41	1.21	21.24	3.59	0.72
M300	A	66.8	0	17.5	5	0	0	9.9	0.8	0	0	4.311	5.000	1.160	24.34	43.86	55.66	0.967	1.18	0.97	33.43	13.98	1.14	16.67	3.05	0.74
	B	67.0	0	17.6	4.4	0	0	10.1	0.9	0	0	10.200	4.159	1.196	12.87	22.99	42.16	0.957	0.46	1.03	36.29	15.38	1.16	22	2.82	0.26
	C	68.8	0	16.6	3.3	0	0	10.6	0.6	0	0	10.200	4.085	1.216	21.03	40.31	52.13	0.968	0.88	0.98	34.8	15.82	1.15	16.69	2.81	0.17
	D	66.4	0	18.4	5.2	0	0	9.3	0.7	0	0	10.000	4.334	1.160	22.4	37.6	48.4	0.968	0.72	0.99	32.59	11.72	1.13	86.08	11.98	0.38
	E	66.3	0	17.7	5.3	0	0	9.9	0.8	0	0	4.235	5.082	1.200	19.28	31.72	66.24	0.965	0.86	1.01	35.64	15.79	1.15	90	12.31	n/a
IN625	A	n/a	n/a	n/a	n/a	n/a	n/a	n/a	n/a	n/a	n/a	4.664	5.359	1.149	25.54	38.59	51.89	0.973	1.09	1.00	40.66	11.91	1.23	63.92	11.94	0.88
	B	n/a	n/a	n/a	n/a	n/a	n/a	n/a	n/a	n/a	n/a	4.175	5.112	1.224	23.65	38.59	51.94	0.962	1.00	0.85	43.91	14.39	1.24	60.1	10.96	n/a
	C	n/a	n/a	n/a	n/a	n/a	n/a	n/a	n/a	n/a	n/a	4.285	5.159	1.204	22.77	37.94	50.75	0.968	1.05	0.94	41.67	17.04	1.24	49.46	8.36	0.82
	D	n/a	n/a	n/a	n/a	n/a	n/a	n/a	n/a	n/a	n/a	4.229	5.074	1.200	27.59	38.45	49.89	0.962	1.01	1.01	44.88	19.63	1.25	90	11.94	1.14

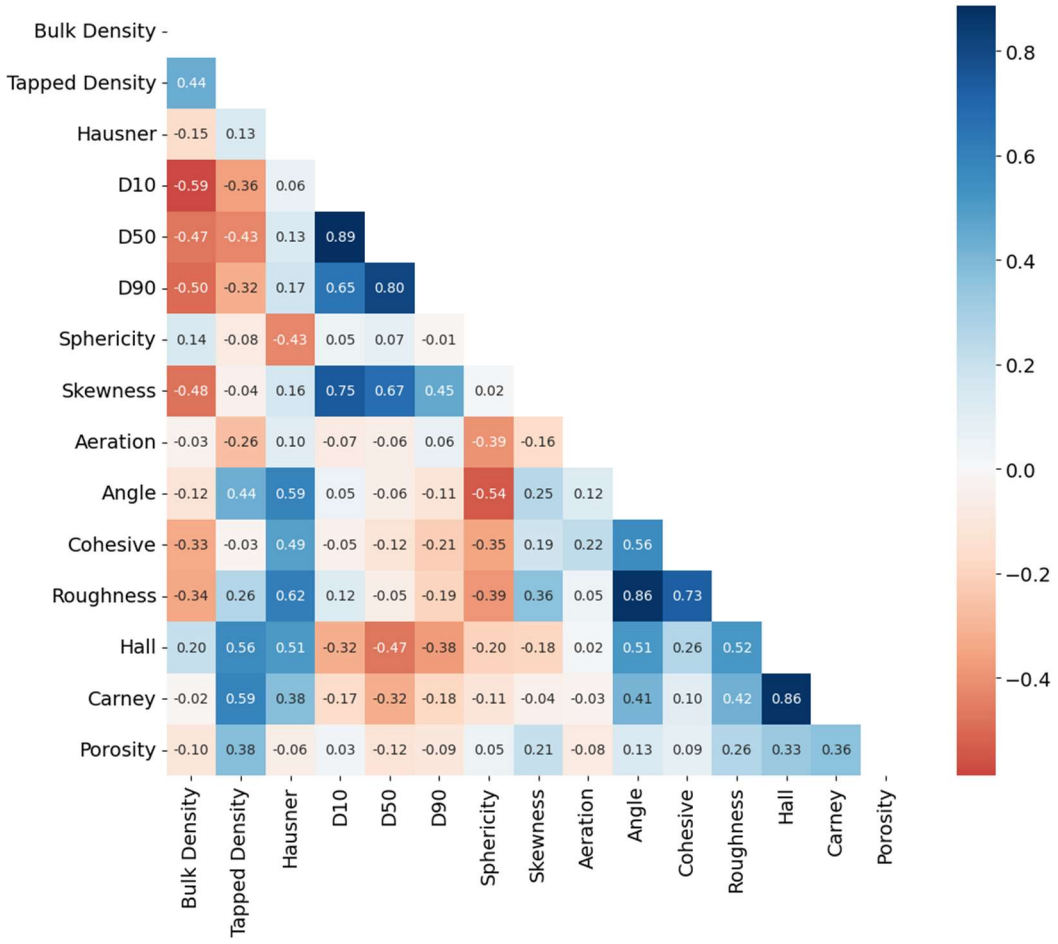

Figure 4. Spearman correlation matrix showing the two-way correlations among powder characteristics.

After Bootstrap sampling was performed on the normalized dataset, it was used for training a gradient-boosting regression ML model. The model was able to predict the response with an accuracy of 87%. Figure 5 shows the comparison between the predicted and actual values for the testing data. The scatter plot showcases the model's predictive capability, where points lying close to the diagonal line (y = x) represent accurate predictions. The clustering of points around this line highlights the quantitative accuracy score, validating the effectiveness of the gradient-boosting regression model in this context.

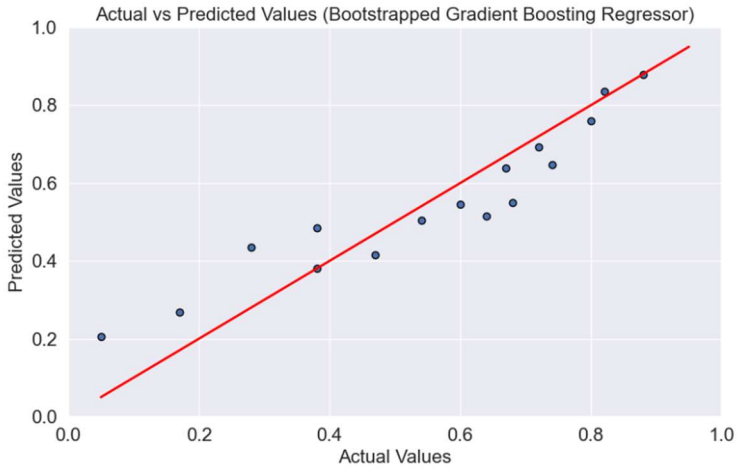

Figure 5. Actual vs predicted responses by the gradient boosting regression model.

4. Conclusions

In this study, we examined alloy powders from various manufacturers to investigate the relationships among powder characteristics and to develop a predictive model for the properties of fabricated parts, specifically focusing on porosity. The characteristics measured included Hall and Carney flowabilities, elemental composition, cohesive index, dynamic angle of repose, roughness index, aeration, tapped density, particle size distribution, and morphology. The tested alloys comprised nine different stainless-steel 316L powders, eight different IN625 powders, seven different M300 maraging steel powders, and six different AlSi10Mg powders. Small cubes were Area Printed using a wide range of laser parameters, and their densities were measured to establish correlations between powder characteristics and part density. The findings revealed both positive and negative correlations between these characteristics and the density of the parts, as well as among the powder characteristics themselves. These correlations help identify the most significant powder properties influencing part properties, depending on the application. This knowledge can reduce the amount of powder testing and experimentation needed for qualification by allowing predictions of certain properties based on those that are highly correlated. Future work will expand the model to include pore morphology and mechanical properties as additional responses, thereby enhancing the robustness of the predictive model. Additionally, the recyclability of different powders will be examined and correlated with their other properties.

References:

[1] C.Y. Yap, C.K. Chua, Z.L. Dong, Z.H. Liu, D.Q. Zhang, L.E. Loh, S.L. Sing, Review of selective laser melting: Materials and applications, Appl Phys Rev 2 (2015) 1–21. https://doi.org/10.1063/1.4935926.

[2] B. Fotovvati, S. Shrestha, N. Ferreri, N. Duanmu, Experimental and Computational Study of Area Printing™ Additive Manufacturing: Inconel 718 and M300 Maraging Steel Density Improvement, Solid Freeform Fabrication Symposium (2023), 1080-1093.

[3] R. Douglas, R. Lancaster, T. Jones, N. Barnard, J. Adams, The Influence of Powder Reuse on the Properties of Laser Powder Bed-Fused Stainless Steel 316L: A Review, Adv Eng Mater (2022). https://doi.org/10.1002/adem.202200596.

[4] S.E. Brika, M. Letenneur, C.A. Dion, V. Brailovski, Influence of particle morphology and size distribution on the powder flowability and laser powder bed fusion manufacturability of Ti-6Al-4V alloy, Addit Manuf 31 (2020). https://doi.org/10.1016/j.addma.2019.100929.

[5] R. Groarke, C. Danilenkoff, S. Karam, E. McCarthy, B. Michel, A. Mussatto, J. Sloane, A.O. Neill, R. Raghavendra, D. Brabazon, 316l stainless steel powders for additive manufacturing: Relationships of powder rheology, size, size distribution to part properties, Materials 13 (2020). https://doi.org/10.3390/ma13235537.

[6] A. Mussatto, R. Groarke, A.O. Neill, M. Ahmed, Y. Delaure, D. Brabazon, Influences of powder morphology and spreading parameters on the powder bed topography uniformity in powder bed fusion metal additive manufacturing, Addit Manuf 38 (2021) 101807. https://doi.org/10.1016/j.addma.2020.101807.

[7] M.A. Spurek, L. Haferkamp, C. Weiss, A.B. Spierings, J.H. Schleifenbaum, K. Wegener, Influence of the particle size distribution of monomodal 316L powder on its flowability and processability in powder bed fusion, Progress in Additive Manufacturing 7 (2022). https://doi.org/10.1007/s40964-021-00240-z.

[8] C. Pleass, S. Jothi, Influence of powder characteristics and additive manufacturing process parameters on the microstructure and mechanical behaviour of Inconel 625 fabricated by Selective Laser Melting, Addit Manuf 24 (2018). https://doi.org/10.1016/j.addma.2018.09.023.

[9] M. Mehrabi, J. Gardy, F.A. Talebi, A. Farshchi, A. Hassanpour, A.E. Bayly, An investigation of the effect of powder flowability on the powder spreading in additive manufacturing, Powder Technol 413 (2023). https://doi.org/10.1016/j.powtec.2022.117997.

[10] A. Averardi, C. Cola, S.E. Zeltmann, N. Gupta, Effect of particle size distribution on the packing of powder beds: A critical discussion relevant to additive manufacturing, Mater Today Commun 24 (2020). https://doi.org/10.1016/j.mtcomm.2020.100964.

[11] https://www.seurat.com/area-printing.

[12] T. Delacroix, F. Lomello, F. Schuster, H. Maskrot, J.P. Garandet, Influence of powder recycling on 316L stainless steel feedstocks and printed parts in laser powder bed fusion, Addit Manuf 50 (2022). https://doi.org/10.1016/j.addma.2021.102553.